Localized charges in thin films by Kelvin probe force microscopy: from single to multiple charges

A. M. Somoza[1] and E. Palacios-Lidón[1,*]

[1] *Departamento de Física – CIOyN, Universidad de Murcia, Murcia 30100, Spain*

(Dated: February 19, 2020)

Abstract

The study of thin film materials is a subject of growing interest. Some of these materials are insulating due to the presence of disorder, which also produces localization of charges. Kelvin probe force microscopy is unique tool to characterize these materials, but a full quantitative interpretation of the results is still lacking. To address this problem, we propose a simple and fast procedure based on the image charge method that represents an advance in this direction since it is not limited to any film thickness or nature of the underlying substrate. Even more, it can be combined with FFT algorithms to generate theoretical images from known charges distributions or to obtain charges distributions from the Kelvin voltage images. Within this framework, we analyze the problem of the lateral resolution of the technique, providing a criterion to estimate it. Finally we address the problem of systems with hopping conductivity where multiple localized charges coexist. We demonstrate that even in these complex systems, the KPFM gives valuable information, allowing to distinguish between non-interacting and interacting electronic systems. Furthermore, it is possible to calculate the charge density in the non-interacting case.

I. INTRODUCTION

The characterization of localized charges on insulating surfaces is a key point in many fields ranging from triboelectric charging studies [1, 2], defects in solids [3–5], nanoclusters [6–8] to biological systems such as adsorbed molecules on dielectric substrates [9, 10]. Moreover, the development of smaller, faster and eco-friendly optoelectronic devices lies on the use of thin films of novel materials such as conducting polymers, low- and high-κ materials or $2D$ flake-like materials such as graphene oxide (GO), reduced GO, transition metal dichalcogenides (TMDCs), etc. These materials usually present low or moderate conductivity and are treated as low-crystallinity or glassy systems in which the high degree of disorder induces the localization of the electron wave function, being their conductivity via hopping mechanisms [11–15]. In these systems, a direct observation of the charge distribution would be of great importance. It could permit to map the energy landscape and could give quantitative validity to the theoretical models. Similarly, the possibility of monitoring the charge dynamics, both in equilibrium as well as when the system is perturbed is fundamental to

* Corresponding author: elisapl@um.es

link the conductivity with the microscopic parameters and it would help to elucidate the role of the different underlying processes.

Kelvin probe force microscopy (KPFM) has been revealed as a unique tool to monitor localized charges [16, 17]. It can give invaluable information inaccessible with other techniques, since it can be used in highly insulating samples [12]. Independently of experimental KPFM mode: amplitude modulation (AM), frequency modulation (FM) or heterodyne mode in static, open-loop, or closed-loop configuration the KPFM signal V_{KPFM} is

$$V_{\mathrm{KPFM}} = V_{\mathrm{Charge}} + V_{CPD} \tag{1}$$

where $V_{CPD} = \Delta\phi/e$ is the classical surface contact potential difference of the electrodes work functions $\Delta\phi$ (tip and sample in this case), and V_{Charge} is the term that includes the localized charges contribution [18]. The quantitative analysis of the V_{Charge} signal is not straightforward and demands a further theoretical modeling. On the one hand, it depends of the tip geometry, the tip-sample distance (z) as well as on the relative permittivity ($\varepsilon_r = \varepsilon/\varepsilon_0$) of the different materials of the system. Thus, all these parameters should be characterized during the data acquisition. On the other hand, the absence of analytical expressions, even for the simplest systems forces to address the problem numerically. This may require a large computational effort, specially when many charges are involved.

Recently, it was shown that this computation can be drastically reduced by using Fast Fourier Transform (FFT) algorithms, both to generate the theoretical $V_{\mathrm{Charge}}(x, y, z)$ image of a pre-established charge distribution or to directly obtain the charge distribution $q(x, y)$ from an experimental $V_{\mathrm{Charge}}(x, y, z)$ image [19]. However, in both cases, the Kelvin voltage image that would generate a point charge placed at the center of the image ($V_{\mathrm{point}}(x, y, z)$), for a specific system and working conditions is needed. Simple charge distributions in thick dielectrics for different tip geometries has been already modeled using different approximations [7, 20–23]. Nevertheless, a model to calculate the V_{point} for localized charges in thin films supported on metallic or dielectric substrates is still lacking.

In this work we propose a simple and fast procedure based on the image charges method to obtain the V_{point} signal when the charges are localized in thin films. This versatile method is not limited to any film thickness or nature of the underlying substrate, and it shows that V_{point} is a key quantity that plays an important role in any quantitative interpretation of V_{Charge} images. We then combine the obtained V_{point} with FFT algorithms to generate the

expected V_{Charge} images for known charges distributions and discuss the final lateral resolution of the technique. Finally, we address the problem of systems with hopping conductivity where multiple localized charges coexist. We demonstrate that even in these complex systems, the KPFM gives valuable information, allowing to distinguish between non-interacting and interacting electronic systems. Furthermore, it is possible to calculate the charge density in the non-interacting case as well as to validate different models for the electron-electron interaction, in the interacting systems.

II. MODEL DESCRIPTION

In order to simplify the following discussion, from now, we will focus on the V_{Charge} contribution of the V_{KPFM} signal considering $V_{CP} = 0$. Following notation of Ref. [18, 23], the electrostatic energy of the tip-sample system in presence of charges is

$$W_{elec}(V, z) = u_0(z) + u_1(z)V + u_2(z)V^2 \tag{2}$$

where V is the bias voltage between tip and sample. The term proportional to V, $u_1(z)$, is due to the interaction of the localized charges with the potential generated by the tip-sample capacitor while the term $u_2(z)$ is the energy of the capacitor, that is independent of the localized charges. Depending on whether the force or the frequency are used for the KPFM measurements, the V_{Charge} signal is

$$V^{AM}_{Charge} = -\frac{u_1'(z)}{2u_2'(z)} \tag{3}$$

$$V^{FM}_{Charge} = -\frac{u_1''(z)}{2u_2''(z)} \tag{4}$$

Therefore, in order to obtain V_{Charge}, the derivatives of $u_1(z)$ and $u_2(z)$ (with respect to z) should be calculated. The image charge method has been previously used to calculate both u_1' and u_2' for systems with localized charges in thick dielectrics, modeling a metallic spherical tip in front of a semi-infinite dielectric[17, 23, 24]. The case of thin films has already been considered in Refs. [25–27], but only the u_2 term was obtained. However, to fully solve the problem of localized charges on thin films, the u_1 term is of vital importance and should be also obtained.

According to the superposition principle a general $V_{\text{Charge}}(x, y, z)$ can be expressed as

$$V_{\text{Charge}}(x, y, z) = \int dx'dy'dz'\ q(x', y', z')V_{\text{point}}(x, y, z; x', y', z'), \tag{5}$$

where $q(x', y', z')$ is the charge density of the problem and $V_{\text{point}}(x, y, z; x', y', z')$ is the V_{Charge} image corresponding to a single point charge located at (x', y', z'). This expression can be further simplified if we assume that all localized charges are located at the same height $z' = d$. Then, as explained in Ref. [19], we can use FFT algorithms:

$$V_{\text{Charge}}(x, y) = \text{IFT}\left(q(\mathbf{k})V_{\text{point}}(\mathbf{k})\right) \tag{6}$$

$$q(x, y) = \text{IFT}\left(V_{\text{Charge}}(\mathbf{k})/V_{\text{point}}(\mathbf{k})\right), \tag{7}$$

where IFT corresponds to Inverse Fourier Transform. We see that we can use $V_{\text{point}}(\mathbf{k})$ either to construct the expected V_{Charge} image from a known charge density $q(x, y, d)$ or to determine it from an experimental V_{Charge} image. The assumption of charges at the same height is reasonable in many experiments where the V_{point} signal is similar for not very different charge heights, such as deposition of charged particles on the surface or in very thin $2D$ materials. There is no a generic formula to know "a priori" the validity of this approximation, and the dependence of the V_{point} with the tip height should be computed for each specific system (see section II and Fig. 2 (c) and (d)). However a generic rule can be given: the lower ε_1 and ε_2 the better the approximation. In the opposite limit, when the V_{point} signal strongly decreased with the charge depth (large ε_1 and/or ε_2), the KPFM technique is only sensitive to the upper charges, and the "'same height"' approximation is still useful to determine the density of these upper charges. For simplicity, in this work we will only consider the case where Eqs. (6,7) are valid, although a generalization to the case of charges located at different planes is straightforward and is described in the Supplemental Material [28].

A. Calculation of V_{point} in thin films materials

Form the previous section it is realized that $V_{\text{point}}(x, y, z, x', y', z')$ plays a key role in the interpretation of V_{charge} images. This quantity had been calculated for thick dielectric, but it has not been estimated for the important case of thin film geometry. Thus, in this section we solve the electrostatic problem, Eqs. (2-4), for a single point charge inside a thin film. A scheme of our system is shown in Fig. 1. A metallic spherical tip (of radius R at constant potential V) is placed (at a tip-surface distance z) on top of a thin layer of thickness h and relative permittivity ε_1 supported by a semi-infinite substrate with relative permittivity ε_2.

Then, a point charge q_0 is placed inside the layer (at $z = d \leq 0$).

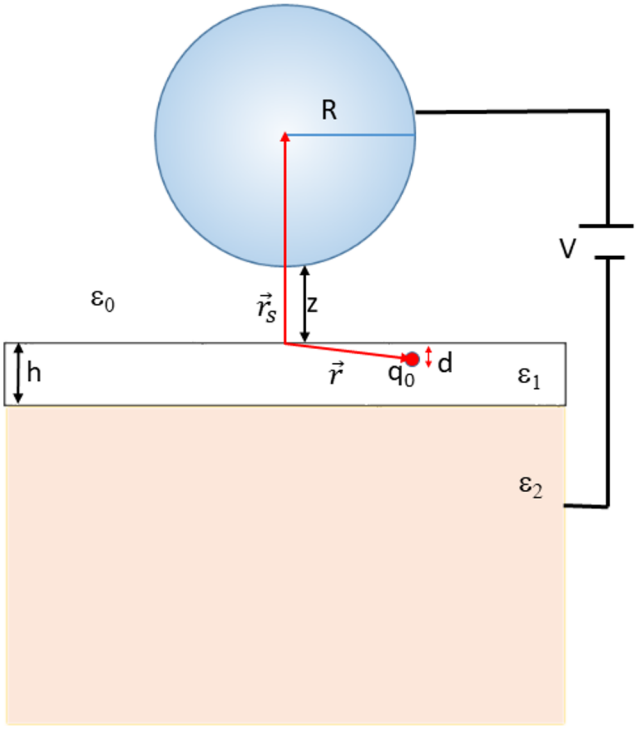

Figure 1. Scheme of the used model

Since we are interested in calculating the force acting on the sphere due to electrostatic interactions, we need to properly describe the electrostatic potential in the region of ε_0. This is done, using the image charge method, by locating image charges inside the sphere and in the sub-surface ($z < 0$) region. To do so, we first calculate the capacitance related u_2 term in a similar way to Ref. [25, 27] but we generalize the result to any ε_2 and not only to metal substrates (we recover their results when $\varepsilon_2 \to \infty$).

In order to calculate the image charges, the general problem is divided in two parts. First, due to the layer geometry and the two boundary conditions that need to be fulfilled (at $z = 0$ and $z = -h$) any charge q located at $z_0 > 0$ will produce an infinite set of image charges in the region $z < 0$ according to the Table I, where $s_1 = (\varepsilon_1 - 1)/(\varepsilon_1 + 1)$ and $s_2 = (\varepsilon_2 - \varepsilon_1)/(\varepsilon_2 + \varepsilon_1)$. Second, to guarantee constant potential at the surface of the sphere, any charge q located at $\mathbf{r}$ outside the sphere will produce an image charge q' located

Table I. Image charges associated to a charge q located at $z_0 > 0$

i	q_i	z_i
$i = 0$	-$s_1 q$	-z_0
$i \geq 1$	$(-s_1)^{i-1} s_2^i (s_1^2 - 1) q$	$-z_0 - 2ih$

at $\mathbf{r}'$, inside the sphere, according to the equations:

$$q' = q \frac{R}{|\mathbf{r}_s - \mathbf{r}|} \tag{8}$$

$$\mathbf{r}' = \mathbf{r}_s + \frac{R^2}{|\mathbf{r}_s - \mathbf{r}|^2} (\mathbf{r} - \mathbf{r}_s) \tag{9}$$

where $\mathbf{r}_s$ is a vector pointing to the center of the sphere.

According with these equations we calculate all the image charges proportional to V; starting the procedure with a point charge $Q_0 = 4\pi\varepsilon_0 RV$, located at the center of the sphere, that produces the desired potential at the sphere surface. Then, equations of Table I must be applied to this charge, producing an infinite set of image charges located at $z < 0$. Each of these charges will generate a new image inside the sphere, which again will produce another infinite set inside the dielectrics, and so on. This results in infinite series of infinite charges, both in the sphere and at $z < 0$, that must be truncated to afford the numerical calculation. Afterward, the image charges inside the sphere are used to calculate the u_2 term [27, 29]. As $Q_V = CV$, u_2 is directly obtained

$$u_2(z) = -\frac{1}{2} C(z), \tag{10}$$

where Q_V is the sum of all the charges proportional to V inside the sphere and V is the potential of the battery connected to the sphere.

Now, to obtain u_1, we need to extend the image charge method to describe to a localized charge inside the thin layer. As shown in the Supplemental Material [28] (see, also, references [25–27] therein), one charge q_0 located at $-h \leq d \leq 0$ will generate two infinite sets of image charges in the $z < 0$ region, as indicated in Table II. Each of these charges will generate new image charges inside the sphere and in $z < 0$ that as in the previous case are calculated with Table I and Eq. (9), all of them proportional to the initial charge q_0.

The computation of the force between all charges inside the sphere with all charges outside directly leads the force acting on the sphere ($-u_1'$ and $-u_2'$). Unfortunately, as stated above,

Table II. Image charges associated to a charge q_0 located at $-h < d < 0$

i	q_i	z_i
$i \geq 0$	$(-s_1 s_2)^i (1-s_1) q_0$	$d - 2ih$

j	q_j	z_j
$j \geq 0$	$-(-s_1 s_2)^j (1-s_1) s_2 q_0$	$-(d + 2(j+1)h)$

for thin layers we are dealing with an extremely large number of charges that results in a large computational effort (for large ε_1 and ε_2, if high precision is required, the number of image charges can be larger than 10^8). To solve this problem, a practical solution (similar to the one used for u_2) is used to calculate u_1 directly, and then calculate the derivative numerically. As shown in Ref.[30], the electrostatic energy of the problem (including the battery) can be written as:

$$U_{\mathit{eff}} = \frac{1}{2} q_0 V(\mathbf{r}) - \frac{1}{2} Q^{tot} V, \tag{11}$$

where $V(\mathbf{r})$ is the electrostatic potential at the location of the charge q_0 and Q^{tot} is the total charge in the sphere. The charge Q^{tot} has two contributions: (i) The sum of all the charges proportional to V inside the sphere (Q_V), and (ii) the sum of all the charges proportional to q_0 inside the sphere (Q_{q_0}). As shown above, the first contribution produces a V^2 dependence and is used to calculate u_2. The potential $V(\mathbf{r})$ also has two contributions: (i) $V_V(\mathbf{r})$, the potential generated by all charges proportional to V, and (ii) $V_{q_0}(\mathbf{r})$, the potential generated by all charges proportional to q_0 (except q_0 itself). Collecting the contributions proportional to V we get

$$u_1 V = (1/2) q_0 V_V(\mathbf{r}) - (1/2) Q_{q_0} V, \tag{12}$$

but it turns out that both terms produce identical contributions [30] so,

$$u_1 = -Q_{q_0}. \tag{13}$$

In summary, not only u_2 but also u_1 can be obtained by adding the different image charges inside the sphere. This result is of great importance for the numerical calculation. We not only save computing time, avoiding the double sum that a direct calculation of forces would require, but also, during the numerical calculation we can save computer memory deleting all charges for which their corresponding images have been taken into account. It also justifies a simple truncation procedure of the infinite series neglecting any image charge smaller and err $\times\, q_0$, where we used typically err $< 10^{-13}$.

Finally, once the u_1 and u_2 for different tip distances are computed, we calculate the derivatives numerically in order to obtain the corresponding V^{AM}_{point} and V^{FM}_{point} from Eq. (4). In this way, typical V^{FM}_{point} curves (horizontal or lateral profiles), with absolute error lower than 10^{-6}, can be computed with a common modern laptop in a few seconds. We will be pleased to share our code under request.

From now on, we will focus on the $V^{FM}_{Charge} = V_{Charge}$ signal; since in our model, the spherical tip assumption neglects the cone and cantilever contributions, and it is well known that V^{FM}_{Charge} is less sensitive to them than the V^{AM}_{Charge} one [31]. A similar analysis could be done for the V^{AM}_{Charge} signal. Finally, We would like to note, that in this work the contribution of u_0 is not used, but according to Eq. (11), it can also be easily calculated if needed, adding the potential generated at $\mathbf{r}$ by all charges proportional to q_0 .

III. RESULTS

A. Model applications

It is not the aim of this work to exhaustively explore and analyze all the possible systems but to show the potential of the proposed method, specially for complex multiple point charges distributions. However, to show its versatility, some relevant examples has been calculated in Fig. 2, where V_{point} of a point charge as a function of the tip-sample distance together with the corresponding lateral profiles at $z = 0.5R$ for different configurations are plotted.

Figure 2 (a) and (b) show the dependence of V_{point} with the film thickness h. Another important case is when the localize charge is not at the surface but buried within the thin layer as shown in Figure 2 (c) and (d). In this situation, depending on the depth of the charge, d, V_{point} may increase or decrease with the tip-sample distance. However, for a fixed distance the deeper the charge, the smaller the V^{FM}_{point} signal is (Fig. 2 (d)). This means that, in systems with localized charges at different depths, the main contribution to the V_{Charge} will come from the upper charges. Finally, changing ε_1 with respect to ε_2 (see Fig. 2 (e)) V_{point} decreases for short distances and increases for large distances with a minimum at $z \approx R$. Besides that, other behaviors can be found for different parameters combinations; the previous results highlight that not only h, d and ε_1, but also z and the ε_2 of the underlying

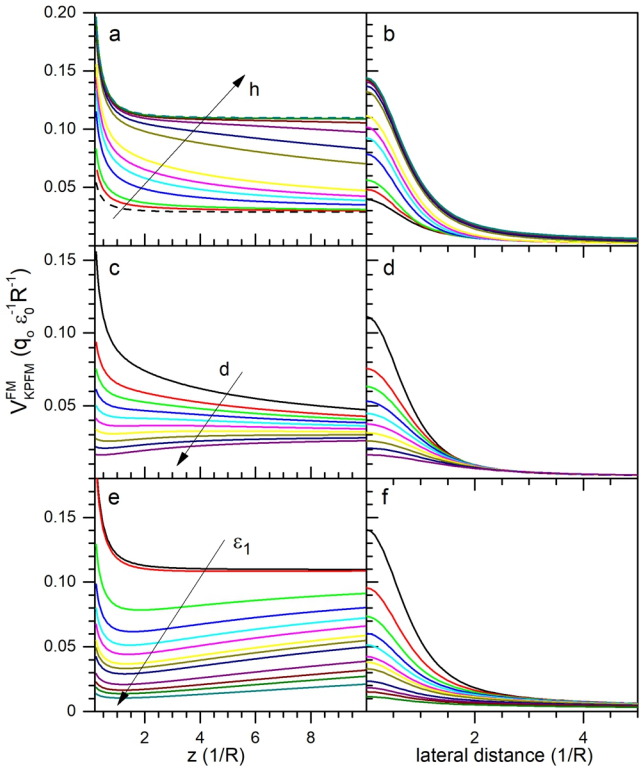

Figure 2. (left graphs) V^{FM}_{Charge} as a function of the tip-sample distance z. (right graphs) Lateral profiles at $z = 0.5R$ (a) and (b) $\varepsilon_1 = 3.9$, $\varepsilon_2 = 12$, $d = 0$ and $h = 0.05, 0.1, 0.3, 0.5, 0.7, 1, 3, 5, 10, 20$ and 50 (R units). The two limits $h = 0$ and $h = \infty$ has been included (dashed lines). (c) and (d) $\varepsilon_1 = 3.9$, $\varepsilon_2 = 12$, $h = 1$ and $d = 0, 0.2, 0.3, 0.4, 0.5, 0.6, 0.7, 0.8, 0.9, 1$ in R units.(e) and (f) $\varepsilon_2 = 3.9$, $h = R$ $d = 0$ and $\varepsilon_1 = 3.9, 4, 6, 8, 10, 12, 15, 17, 20, 30, 40, 50, 70$.

substrate, greatly affect the contrast of the V_{Charge} images. While the former are usually related with the studied thin film material, the latter can be tuned (selecting the appropriate substrate) to optimize the KPFM measurements.

B. V_{Charge} images generation and lateral resolution

From the lateral profiles shown above and taking advantage of the uniaxial symmetry, we directly obtain the V_{point} image for a specific system (ε_1, ε_2, h and d) and measurement parameters (R, z, image size $L \times L$ and image number of points $n \times n$). Then, by using Eq. (6) we generate a theoretical $V_{\text{Charge}}(x, y, z)$ image produced by an "ad-hoc" charge distribution, $q(x, y)$ [19]. In order to show this procedure, two V_{point} calculated for the

same system ($h = R = 15$ nm, $d = 0$, $\varepsilon_1 = 3.9$, $\varepsilon_2 = 12$, $L = 600$ nm) but at different tip-sample distances ($z = 7$ nm and 28 nm) are used to obtain the corresponding V_{Charge} images of a charge distribution consisting of three pairs of charges separated 7, 14 and 28 nm respectively (Fig. 3 (a) and (b)). This simple example is useful to address the

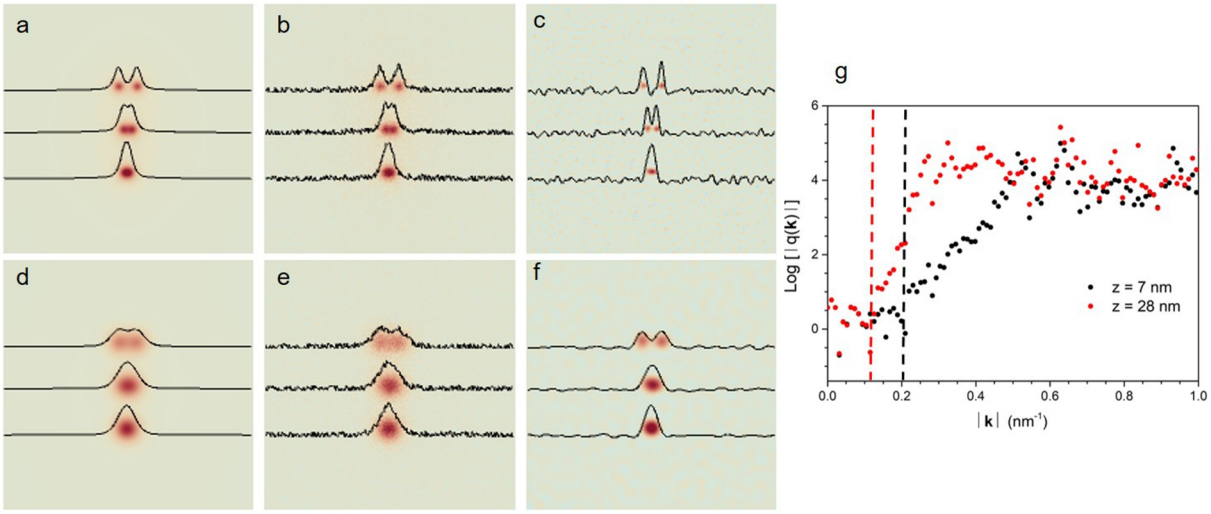

Figure 3. (a) Generated V_{Charge}^{FM} image of $q(x, y)$ of three pairs of charges separated 7, 14 and 28 nm in a system with parameters $h = R = 15$ nm,$d = 0$, $\varepsilon_1 = 3.9$, $\varepsilon_2 = 12$, $L = 600$ nm and $z = 7$ nm, (b) Simulated experimental images with a random Gaussian noise ($\sigma = 15$ mV), (c) $q(x, y)$ image obtained after IFT deconvolution with k_c give by Eq. (17). (d),(e) and (f) Same images as (a), (b) and (c) but obtained at $z = 28$ nm, (g) $q(\mathbf{k}) = \frac{V_{\text{Charge}}(\mathbf{k})}{V_{\text{point}}(\mathbf{k})}$. The dashed vertical lines indicated the k_c used in each of the cases.

lateral resolution question, that in any KPFM experiment is typically discussed directly from V_{KPFM} profiles. In presence of localized charges, this lateral resolution is directly related to the broadness of the corresponding V_{point} and mainly depends on the measurement parameters (R and z) [17]. However, it is important to note that a better lateral resolution can be achieved by analyzing the $q(x, y)$ image that is obtained from Eq. (7). A noisy experimental V_{Charge} image can be expressed as

$$V_{\text{Charge}}(x, y, z) = V_{\text{Charge}}^{ideal}(\text{x}, \text{y}, \text{z}) + \sigma^{\text{noise}}(\text{x}, \text{y}) \tag{14}$$

where $V^{ideal}_{\rm Charge}(\mathrm{x},\mathrm{y})$ is the ideal noise-free image generated by an underlying charge distribution while $\sigma^{noise}(\mathrm{x},\mathrm{y})$ is the noise matrix. Then,

$$q(x,y) = IFT\left(\frac{V^{ideal}_{\rm Charge}(\mathbf{k}) + \sigma^{noise}(\mathbf{k})}{V_{\rm point}(\mathbf{k})}\right) \tag{15}$$

In an ideal noise-free image ($\sigma^{noise} = 0$), Eq. (15) would lead to the exact charge distribution. In practice, the final lateral resolution of the $q(x,y)$ image is limited by the cut-off, k_c, of the filter applied to $(V^{ideal}_{\rm Charge}(\mathbf{k}) + \sigma^{noise}(\mathbf{k}))/V_{\rm point}(\mathbf{k})$ needed to avoid non-physical artifacts produced by different sources of noise [19]. This cutoff determines the real lateral resolution, δx, that can be achieved, as it is roughly half of the wavelength related to k_c:

$$\delta x \approx \frac{\pi}{k_c}. \tag{16}$$

This k_c can be easily estimated from Eq. (15) (see also Fig. 3 (g)). If the main source of noise is white noise, $\sigma^{noise}(\mathbf{k})$ is approximately constant in amplitude while $V_{\rm point}(\mathbf{k})$ decays exponentially with k (as it does $V^{ideal}_{\rm Charge}(\mathbf{k})$). So a good estimation of k_c is obtained from the ratio

$$\frac{\sigma^{noise}(k_c)}{V_{\rm point}(k_c)} \approx 1. \tag{17}$$

Actually, under an appropriated data filtering this resolution can be slightly improved [19]. These ideas are shown in Fig. 3 (b) and (e), where experimental images has been simulated by adding a random Gaussian noise to each image point of Fig. 3 (a) and (d). In order to obtain the corresponding $q(x,y)$ images (Fig. 3(c) and (f)), the cut-off radius has been used in each case following the previous criterion. In Fig. 3 (g) it can be observed how the apparent $q(\mathbf{k})$ grows exponentially after the dashed line due to the effect of $\sigma^{noise}(\mathbf{k})$ (the flat behavior for large k is due to numerical errors).

C. Multiple-charges distributions: effect of charge correlations

The previous methodology allows us to address the study of systems where multiple charges coexist [1, 2, 32–34]. In this section we will focus on thin-film systems with hopping conductivity where charge localization plays a crucial role [11–15]. These systems are characterized by a large amount of disorder that produces the localization of charges and the electronic transport takes place via activated tunneling: electrons hop from a localized

occupied state to an empty one assisted by phonons. Coulomb interaction between charges is especially important in the strongly localized regime because the low mobility of charges results in a drastic reduction of the screening. One significant effect of the interaction is that, at low temperatures, the density of states (DOS) is greatly reduced and a soft gap is opened at the Fermi level, as predicted by Pollak [35] and characterized by Efros and Shklosvkii [36]. In this case conductivity follows an Efros-Shklovskii variable-range hoping (VRH) law. At high temperatures, interactions become less important and as a result the soft gap is filled and conduction changes to a Mott VRH law. In general, we can expect that correlations between charges become negligible when $kT > U$, where U is the typical interaction energy between nearest neighbors localized charges. In order to analyze how the interactions and correlation between charges modify the V_{Charge} images, we have generated correlated and non-correlated $q(x, y)$ distributions using a standard electron glass model [37, 38] considering a squared system of size LxL with N sites randomly distributed.

$$\mathcal{H} = \sum_{i=1}^{N} \epsilon_i n_i + U_0 R \sum_{i<j} \frac{(n_i - K)(n_j - K)}{r_{ij}}, \tag{18}$$

where N is the number of sites. The first term of the right-hand side includes the effect of disorder, n_i is the occupation of one site (which is either 0 or 1) and ϵ_i is a random energy in the interval $[-W/2, W/2]$, where W measures the strength of disorder. The second term corresponds to the Coulomb interaction between sites, where K is the mean occupation of one site (we consider $K = 1/2$). The strength of interaction is determined by $U_0 R$, where R is the tip radius. Then, U_0 corresponds to the interaction energy of two unit charges separated a tip radius, and we will fix it to $U_0 = 1$ as the unit of energy. Although, so far, this analysis must be considered qualitative, we have fixed some quantities to realistic values: $L = 500$ nm, $W = 2U_0$, and the localization length is assumed to be smaller than 2 nm to consider them as point charges in a V_{Charge} image. Finally, to get typical equilibrium configurations of the $q(x, y)$, we performed Monte Carlo simulations using a metropolis algorithm for electron glasses [39]. With this model, we can generate multi-charges distributions for systems both with interacting, correlated charges (we fixed temperature $kT = 0.03U_0$) and with uncorrelated charges (we fixed $U_0 = 0$, although similar results would have been obtained for interacting systems at high temperatures) and therefore compare their expected V_{Charge} images.

An example of how the V_{Charge} images evolve as the number of charges, N, is increased is shown in Fig. 4 ((a)-(d) non-interacting and (e)-(h) interacting systems respectively)

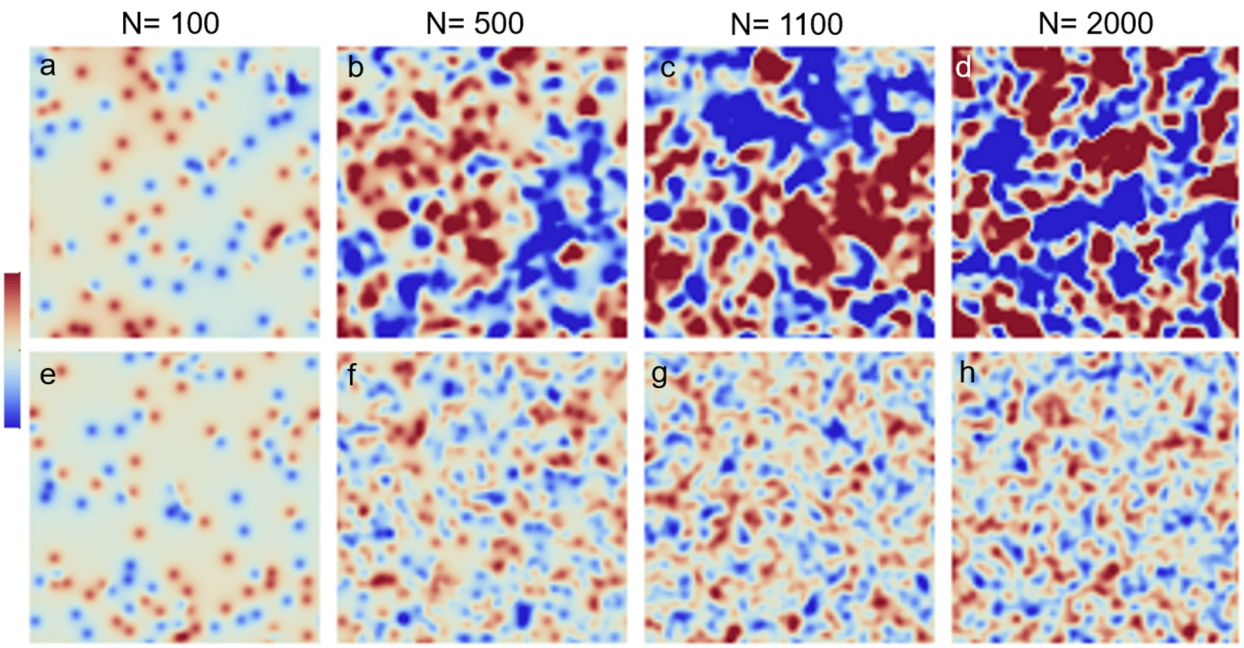

Figure 4. V^{FM}_{Charge} images from $q(x, y)$ with an increasing number of charges generated with the same V_{point} ($\varepsilon_1 = 3.9$, $\varepsilon_2 = 12$, $h = 15$ nm, $R = 15$ nm, $z = 7$ nm, image lateral size $L = 500$ nm for (a)-(d) non-interacting and (e)-(h) interacting systems. To highlight the differences between the two type of systems, the z scale has been fixed to ± 120 mV in all the images

for $\varepsilon_1 = 3.9$, $\varepsilon_2 = 12$, $h = 15$ nm (eg. a 15 nm polymer or SiO_2 on silicon) imaged with a tip of $R = 15$ nm at a tip-sample distance $z = 7$ nm, being the image lateral size $L = 500$ nm. For these parameters, the typical distance between nearest charges corresponds to $\bar{l} = 50, 22, 15, 11$ nm. At low charge densities, the localized charges can be resolved individually and the effect of interaction is almost negligible as the mean distance between particles is large. As N increases (decreasing the mean distance between charges), the V_{Charge} of the non-interacting system develops large bright and dark domains increasing the overall image contrast. On the contrary, in the interacting system, the domain size and domain contrast are basically constant and insensitive to the number of charges, being the V_{Charge} image very similar independently of N. This is understood noticing that, in a non-interacting system ($U_0 = 0$ or $kT \ll U_0$), the probability of charge aggregation of the same sign increases with N and therefore the domain size and contrast of the generated V_{Charge} domains increases. Conversely, in the interacting system ($kT = 0.03U_0$), this possibility is not allowed as charges of the same sign strongly repels each other and tend to be surrounded

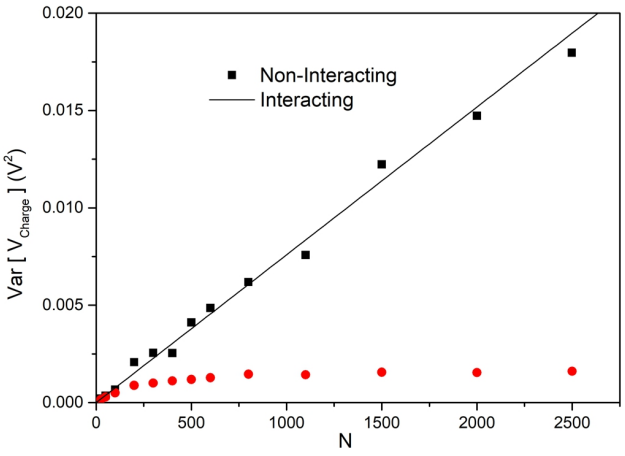

Figure 5. $\mathrm{Var}[V^{FM}_{\mathrm{Charge}}]$ vs N for non-interacting and interacting systems ($\varepsilon_1 = 3.9$, $\varepsilon_2 = 12$, $h = 15$ nm, $R = 15$ nm, $z = 7$ nm). The solid black line correspond to Eq. (19).

by charges of the opposite sign. In this situation, the average local charge should be always about $\pm e$ independently of N. Then, an alternate domain contrast is expected in the V_{Charge} image, being the domain size about the width of the corresponding $V_{\mathrm{point}}(x, y, z)$. The above results show that it is possible to distinguish between interacting and non-interacting systems from the overall appearance and contrast of the V_{Charge} image, as the two kind of systems generate very different images.

According to this discussion we have found that the variance of a V^{FM}_{Charge} image is a sensitive quantity to determine the effect of interactions (see Fig. 5)). This is a simple but interesting quantity also because it is easy to demonstrate that, for the non-interacting case:

$$\mathrm{Var}[V^{FM}_{\mathrm{Charge}}] = N\mathrm{Var}[V_{\mathrm{point}}] + \sigma^2_{noise}, \tag{19}$$

where σ^2_{noise} is the variance of the experimental noise (assumed to be uncorrelated white noise). This relation provides a useful tool to estimate the charge density in non-interacting systems, if the parameters of the system are properly characterized. Verification of the results can be obtained measuring at different tip-sample distances.

The dependence of the $\mathrm{Var}[V_{\mathrm{Charge}}]$ with N in the interacting system is more complicated and it is out of the scope of the present work. However, we note that it is related to charge correlations due to interactions. It strongly depends of the model and the parameters used, as well as on the temperature. Nevertheless, $\mathrm{Var}[V_{\mathrm{Charge}}]$ could be a simple and useful quantity to validate different theoretical interacting models. Also, if V_{point} is well characterized for a

system, the charge correlation function can be obtained from the V_{Charge} image using FFT methods.

IV. CONCLUSIONS

There is no doubt that the KPFM is a very promising technique to study systems with localized charges, but at the same time, it becomes necessary to improve the quantitative interpretation of the results. In this sense, the image generated by a point charge, V_{point}, is a key quantity. On the one hand, it allows to generate theoretical V_{Charge} images to test different physical models. It is also needed in order to calculate the underlying charge distribution from experimental images. In this context, we have proposed a charge image method to calculate it for geometries consistent with most experiments (a layer of thickness h and relative permittivity ε_1 on top of another material with relative permittivity ε_2). Even more, we have analyze the influence of the V_{point} in the lateral resolution as well as the role of the image noise, that is the limiting factor of the final lateral resolution of the technique.

In systems with multiple charges distribution, the V_{Charge} image is always composed of bright and dark potential domains. At large charge densities, each domain cannot be assigned neither to an individual charge nor to an effective charge density. Due to the long-range nature of the electrostatic interaction the V_{Charge} contrast is not only due to the charge below the tip, but the nearby charges have also important contributions. However, even in this situation, the quantification of $\text{Var}[V_{\text{Charge}}]$ makes possible to determine the density of localized charges for non interacting systems, or at least measure the importance of interactions. In addition, working with the $q(x, y)$ images, obtained from the V_{Charge} images by using the V_{point} image calculated with the proposed method would lead to a more accurate analysis. This is particularly important on the study of heterogeneous charges distributions or charge dynamics.

ACKNOWLEDGMENTS

The work was supported by the Spanish MINECO Grants No. FIS2015-67844-R, ENE2016-79282-C5-4-R, and by Fundación Séneca grant 19907/GERM/15 and 20860/PI/18.

[1] H. T. Baytekin, A. Z. Patashinski, M. Branicki, B. Baytekin, S. Soh, and B. A. Grzybowski, Science **333**, 308 (2011).

[2] D. J. Lacks and T. Shinbrot, Nat Rev Chem **3**, 465 (2019).

[3] L. N. Kantorovich, A. L. Shluger, and A. M. Stoneham, Phys. Rev. Lett. **85**, 3846 (2000).

[4] T. Hynninen, A. S. Foster, and C. Barth, e-Journal of Surface Science and Nanotechnology **9**, 6 (2011).

[5] W. Steurer, J. Repp, L. Gross, I. Scivetti, M. Persson, and G. Meyer, Phys. Rev. Lett. **114**, 10.1103/PhysRevLett.114.036801 (2015).

[6] L. N. Kantorovich, A. S. Foster, A. L. Shluger, and A. M. Stoneham, Surface Science **445**, 283 (2000).

[7] T. Mélin, H. Diesinger, D. Deresmes, and D. Stiévenard, Phys. Rev. B **69**, 035321 (2004).

[8] B. Hoff, C. R. Henry, and C. Barth, Nanoscale **8**, 411 (2016).

[9] J. L. Neff and P. Rahe, Phys. Rev. B **91**, 085424 (2015).

[10] M. Salerno and S. Dante, Materials **11**, 951 (2018).

[11] M. Ortuño, E. Escasain, E. Lopez-Elvira, A. M. Somoza, J. Colchero, and E. Palacios-Lidon, Sci Rep **6**, 10.1038/srep21647 (2016).

[12] M. F. Orihuela, M. Ortuño, A. M. Somoza, J. Colchero, E. Palacios-Lidón, T. Grenet, and J. Delahaye, Phys. Rev. B **95** (2017).

[13] B. Muchharla, T. N. Narayanan, K. Balakrishnan, P. M. Ajayan, and S. Talapatra, 2D Mater. **1**, 011008 (2014).

[14] D. Joung and S. I. Khondaker, Phys. Rev. B **86**, 235423 (2012).

[15] U. O. Uyor, A. P. I. Popoola, O. M. Popoola, and V. S. Aigbodion, J Mater Sci: Mater Electron **30**, 16966 (2019).

[16] H. Söngen, P. Rahe, J. L. Neff, R. Bechstein, J. Ritala, A. S. Foster, and A. Kühnle, J. of App. Phys. **119**, 025304 (2016).

[17] S. Sadewasser and T. Glatzel, *Kelvin Probe Force Microscopy: From Single Charge Detection to Device Characterization* (Springer, 2018).

[18] C. Barth, T. Hynninen, M. Bieletzki, C. R. Henry, A. S. Foster, F. Esch, and U. Heiz, New Journal of Physics **12**, 093024 (2010).

[19] J. F. Gonzalez, A. M. Somoza, and E. Palacios-Lidón, Phys. Chem. Chem. Phys. **19**, 27299 (2017).

[20] E. Palleau, L. Ressier, . Borowik, and T. Mélin, Nanotechnology **21**, 225706 (2010).

[21] G. Valdrè, D. Moro, D. Lee, C. Smith, I. Farrer, D. Ritchie, and R. Green, Nanotechnology **19**, 045304 (2008).

[22] C. Riedel, A. Alegría, R. Arinero, J. Colmenero, and J. J. Sáenz, Nanotechnology **22**, 345702 (2011).

[23] M. F. Orihuela, A. M. Somoza, J. Colchero, M. Ortuño, and E. Palacios-Lidón, Nanotechnology **28**, 025703 (2017).

[24] A. Sadeghi, A. Baratoff, S. A. Ghasemi, S. Goedecker, T. Glatzel, S. Kawai, and E. Meyer, Phys. Rev. B **86**, 075407 (2012).

[25] E. Poli, IEEE transactions on magnetics **28**, 1076 (1992).

[26] S. F. Lyuksyutov, R. A. Sharipov, G. Sigalov, and P. B. Paramonov, Exact analytical solution for electrostatic field produced by biased atomic force microscope tip dwelling above dielectric-conductor bi-layer (2004), arXiv:cond-mat/0408247 [cond-mat.mtrl-sci].

[27] A. Sadeghi, A. Baratoff, and S. Goedecker, Phys. Rev. B **88**, 035436 (2013).

[28] See Supplemental Material at URL for charges at different heights and one charge inside a thin slab.

[29] G. M. Sacha, E. Sahagún, and J. J. Sáenz, J. of App. Phys. **101**, 024310 (2007).

[30] L. N. Kantorovich, A. I. Livshits, and M. Stoneham, J. Phys.: Condens. Matter **12**, 795 (2000).

[31] J. Colchero, A. Gil, and A. M. Baró, Phys. Rev. B **64**, 245403 (2001).

[32] V. Albrecht, A. Janke, A. Drechsler, G. Schubert, E. Németh, and F. Simon, in *Characterization of Polymer Surfaces and Thin Films*, Vol. 132, edited by K. Grundke, M. Stamm, and H.-J. Adler (Springer-Verlag, Berlin/Heidelberg, 2006) pp. 48–53.

[33] C. A. Rezende, R. F. Gouveia, M. A. da Silva, and F. Galembeck, Journal of Physics: Condensed Matter **21**, 263002 (2009).

[34] A. Barnes and A. Dinsmore, J. of Electrostatics **81**, 76 (2016).

[35] M. Pollak, Discuss. Faraday Soc. **50**, 13 (1970).

[36] A. L. Efros and B. I. Shklovskii, Journal of Physics C: Solid State Physics **8**, L49 (1975).

[37] B. I. Shklovskii and A. L. Efros, *Electronic Properties of Doped Semiconductors* (Springer Science & Business Media, 2013).

[38] M. Pollak, M. Ortuño, and A. Frydman, *The Electron Glass* (Cambridge University Press, 2013).

[39] D. N. Tsigankov and A. L. Efros, Phys. Rev. Lett. **88**, 176602 (2002)

.